JACS
JOURNAL OF THE AMERICAN CHEMICAL SOCIETY

Article

pubs.acs.org/JACS

Entropy-Driven Pattern Formation of Hybrid Vesicular Assemblies Made from Molecular and Nanoparticle Amphiphiles

Yijing Liu,[†] Yanchun Li,[‡] Jie He,[†] Kaleb John Duelge,[†] Zhongyuan Lu,*[,‡] and Zhihong Nie*[,†]

[†]Department of Chemistry and Biochemistry, University of Maryland, College Park, Maryland 20742, United States

[‡]State Key Laboratory of Theoretical and Computational Chemistry, Institute of Theoretical Chemistry, Jilin University, Changchun 130023, China

Supporting Information

ABSTRACT: Although an analogy has been drawn between them, organic molecular amphiphiles (MAMs) and inorganic nanoparticle (NP) amphiphiles (NPAMs) are significantly different in dimension, geometry, and composition as well as their assembly behavior. Their concurrent assembly can synergetically combine the inherent properties of both building blocks, thus leading to new hybrid materials with increasing complexity and functionality. Here we present a new strategy to fabricate hybrid vesicles with well-defined shape, morphology, and surface pattern by coassembling MAMs of block copolymers (BCPs) and NPAMs comprising inorganic NPs tethered with amphiphilic BCPs. The assembly of binary mixtures generated unique hybrid Janus-like vesicles with different shapes, patchy vesicles, and heterogeneous vesicles. Our experimental and computational studies indicate that the different nanostructures arise from the delicate interplay between the dimension mismatch of the two types of amphiphiles, the entanglement of polymer chains, and the mobility of NPAMs. In addition, the entropic attraction between NPAMs plays a dominant role in controlling the lateral phase separation of the two types of amphiphiles in the membranes. The ability to utilize multiple distinct amphiphiles to construct discrete assemblies represents a promising step in the self-assembly of structurally complex functional materials.

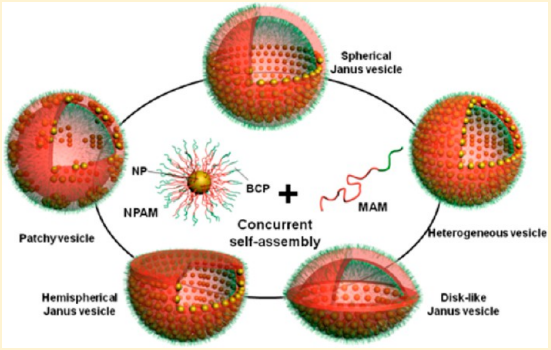

1. INTRODUCTION

Natural or synthetic amphiphiles such as lipids[1] and block copolymers (BCPs)[2] represent one of the most prospective building blocks for constructing functional materials. Molecular amphiphiles (MAMs) can self-assemble into a rich variety of complex hierarchical nanoarchitectures with applications ranging from biomedicine, tissue engineering, to electronics.[3−6]

In contrast, inorganic nanoparticle (NP) amphiphiles (NPAMs) can exhibit intrinsic optical, electronic, and magnetic properties that are unattainable by their organic counterparts.[7−9] NPAMs are usually constructed by synthesizing NPs with distinct hydrophilic and hydrophobic regions or attaching amphiphilic molecules (i.e., BCPs) on the surfaces of inorganic NPs.[8−10] This new class of building blocks can self-assemble as better-studied molecules into defined nanostructures with various morphologies such as chains, micelles, vesicles, and tubules.[7−15] The organization of NPAMs enables one to fine-tune the synergetic coupling between subunits (i.e., semiconducting, metallic, and magnetic NPs) within assemblies,[16] thus fully realizing the enormous potential of NPs in such as biomedicine,[17,18] energy,[19] and optoelectronics.[20]

Recently, the rapidly rising demand for new materials drives the design of nanostructures with increasing complexity and new functionality.[21−26] One promising strategy is to simultaneously assemble multiple types of amphiphiles into discrete architectures. Most examples involve the concurrent assembly of two or more MAMs of lipids, surfactants, and/or polymers.[1,22,27,28] The physical and chemical properties of these assembled structures are inherently limited by the nature of organic species. The combination of organic MAMs and inorganic NPAMs can potentially surpass such limitations of assembled materials by imparting the system with summation or collective properties of all building blocks. However, the concurrent self-assembly of MAMs and NPAMs has rarely been explored, and their coassembly behaviors are still unclear.[29] We hypothesize that the cooperativity and complexity of such system will maximize our capability of creating novel hybrid assemblies with desired architectures and properties.

Here we report an experimental and computational study on the coassembly of BCP amphiphiles and NPAMs comprising inorganic NPs tethered with amphiphilic linear BCPs in selective solvents (Figure 1). The binary mixtures of amphiphiles assembled into a variety of hybrid vesicles with well-defined shape, morphology, and surface pattern by controlling the entropy-driven lateral phase separation of binary amphiphiles within membranes. Typical assembled nanostructures include patchy vesicles (PVs) with multiple

Received: November 29, 2013
Published: January 21, 2014

   dx.doi.org/10.1021/ja412172f | J. Am. Chem. Soc. 2014, 136, 2602−2610

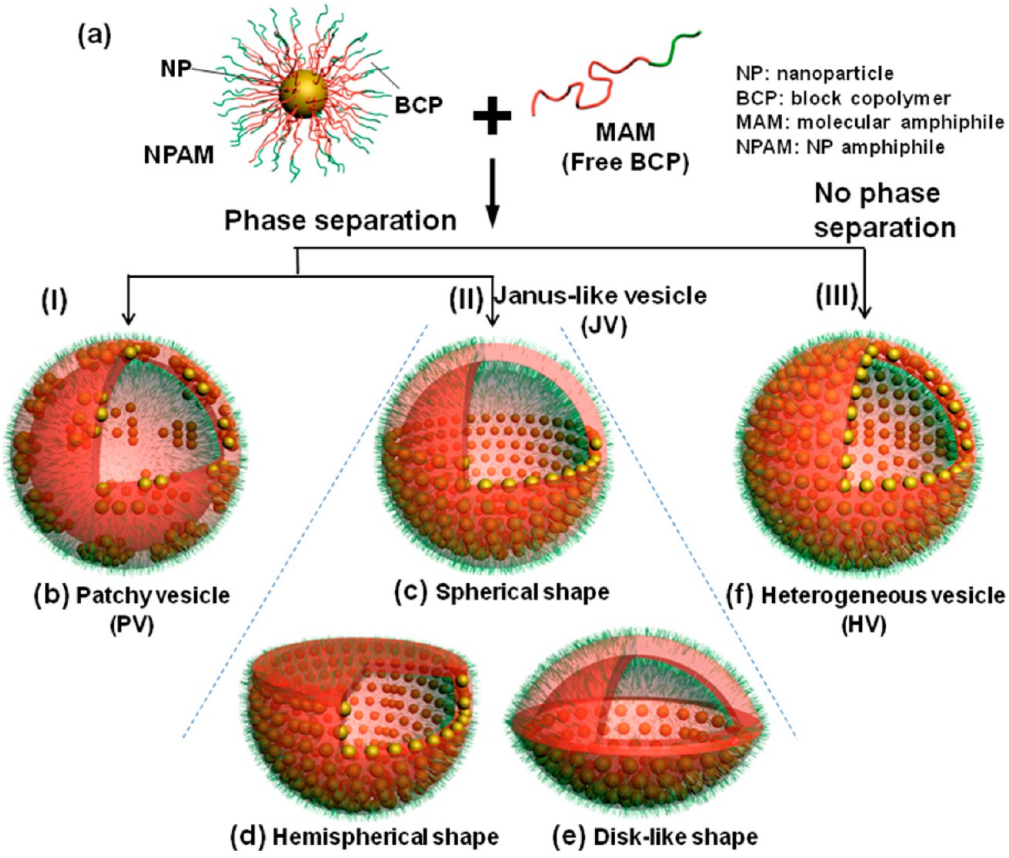

Figure 1. Schematic illustration of the coassembly of binary mixtures of MAMs and NAPAMs into hybrid vesicles with defined shape, morphology and surface pattern. The NPAM consists of an inorganic NP tethered with amphiphilic linear BCPs, while free amphiphilic BCP is used as MAM (a). When phase separation occurs (I and II), the concurrent assembly produces spherical hybrid PVs with multiple NPAM domains (b) and hybrid JVs with distinguished MAM and NPAM halves (c–e). The JVs acquire a spherical (c), hemispherical (d), and disk-like (e) shapes depending on the assembly parameters. When no phase separation occurs (III), the assembly generates HVs with uniform distribution of NPAMs in the membrane (f).

small NPAM domains surrounded by MAM phase (Figure 1b), Janus-like vesicles (JVs) with distinguished MAM and NPAM halves (Figure 1c–e), and heterogeneous vesicles (HVs) with uniform distribution of NPAMs (Figure 1f). The formation of different nanostructures arises from the delicate interplay between the dimension mismatch of the two types of amphiphiles, the entanglement of polymer chains, and the mobility of NPAMs. Additionally, the entropic attraction between NPAMs, as a result of the maximization of the conformational entropy of MAM' BCP chains, plays a dominant role in controlling the phase-separation of the two types amphiphiles in the membranes. It is remarkable that this strategy allows the preparation of hybrid JVs with intriguing nonspherical shapes, including hemispherical (Figure 1d) and disk-like shape (Figure 1e). The ability to directly integrate multiple amphiphiles with significantly different dimensions, geometries, and compositions into discrete nanostructures opens new avenues to fabricate structurally complex hybrid materials with advanced properties.

2. EXPERIMENTS

2.1. Materials. Styrene, azobis(isobutyronitrile) (AIBN), 4-cyano-4-(phenylcarbonothioylthio) pentanoic acid (CPPA), tetrahydrofuran (THF), dimethylformamide (DMF), sodium borohydride ($NaBH_4$, ≥99%), gold(III) chloride trihydrate ($HAuCl_4$, ≥99.9% trace metals basis), sodium citrate tribasic dihydrate (≥99%), hexadecyltrimethylammonium bromide (CTAB), and silver nitrate ($AgNO_3$) were purchased from Sigma-Aldrich. Styrene was distilled under vacuum prior to use and stored in a freezer at −20 °C. AIBN was recrystallized from ethanol. Deionized water (Millipore Milli-Q grade) with resistivity of 18.0 MΩ was used in all the experiments. Polystyrene-*block*-poly(ethylene oxide) (PS-*b*-PEO) (i.e., PS_{307}-*b*-PEG_5, PS_{307}-*b*-PEG_{45}, and PS_{307}-*b*-PEG_{383}) without functional groups was purchased from Polymer Source, Inc.

2.2. Synthesis of Thiol-Terminated BCPs. Thiol-terminated BCPs of HS-PS-*b*-PEO were synthesized using reversible addition–fragmentation chain transfer (RAFT) polymerization reported previously.[11] Chain transfer agent (PEO-CTA) was synthesized by attaching 4-cyano-4-(phenylcarbonothioylthiol) pentanoic acid to the PEO by esterification. RAFT polymerization was performed to grow PS block of BCPs from the PEO-CTA.

2.3. Synthesis of Au NPs (AuNPs) and Gold Nanorods (AuNRs). AuNPs were synthesized using sodium citrate reduction method reported previously.[30] To make 19 nm AuNP, 1 mL of 10 mg/mL $HAuCl_4$ aqueous solution and 3 mL of 10 mg/mL sodium citrate were injected into 500 mL of boiling water under stirring. After refluxing for 30 min, the solution temperature was decreased to 85 °C. Another 3 mL sodium citrate solution and 1 mL of $HAuCl_4$ solution were injected. AuNRs were prepared using seed-mediated growth method as reported.[12] A seed solution was first prepared by mixing 5 mL of 1.0 mM $HAuCl_4$, 2.5 mL of H_2O, and 5.0 mL of 0.2 M CTAB, followed by injecting 0.6 mL of ice-cold 10 mM $NaBH_4$ under stirring. The grow solution was prepared by mixing 1.0 mL of 10 mM $HAuCl_4$, 19.0 mL of 0.1 M CTAB, 0.2 mL of 10 mM $AgNO_3$, and 0.12 mL of 0.1 M ascorbic acid. A 0.32 mL seed solution was added into the growth solution by gently shaking. The solution was then set aside overnight at 28 °C.

2.4. Surface Modification of AuNPs. Briefly, a 2 mg of thiol-terminated BCPs was dissolved in 10 mL of DMF. A 40 mL of

dx.doi.org/10.1021/ja412172f | J. Am. Chem. Soc. 2014, 136, 2602–2610

aqueous solution of AuNPs was concentrated into 100 μL by centrifuge. The concentrated AuNP solution was slowly added into the above BCPs solution in DMF while shaking. Subsequently, the mixture was sonicated for 1 h to avoid aggregation and then was kept undisturbed for 6 h to complete the ligand exchange. To remove free BCPs, the solution was centrifuged for eight times and redispersed in THF. The estimated free BCPs left in the system should be lower than 2×10^{-12} mg/mL.

2.5. Self-Assembly and Characterization. MAMs and NPAMs were dissolved in THF with predetermined concentration. Ultrapure water was added dropwise into the mixture while vigorously stirring, until the final water content reached 25% by volume. The solution was shaken for 5 h and then dialyzed against water using dialysis bags (M_w cutoff of 3000−5000 g/mol) for 24 h to remove THF.

The morphologies of assemblies were imaged using a Hitachi SU-70 Schottky field emission gun scanning electron microscope (FEG-SEM) and a JEOL FEG transmission electron microscope (FEG-TEM). Samples for SEM were prepared by casting a 5−10 μL of NP aqueous solution on silicon wafers and dried at room temperature. TEM samples were prepared by casting 5−10 μL of NP aqueous solution on 300 mesh copper grids covered with carbon film and dried at room temperature.

2.6. Model and Simulation Method. *Mesoscale Simulation Method − Dissipative Particle Dynamics (DPD).* For more details, see the SI. DPD technique is a suitable and efficient method for simulating the self-assembly of BCPs[31,32] and NPs.[33,34] In this method, the time evolution of interacting coarse-grained (CG) beads is governed by Newton's equations of motion as[35]

$$\frac{d\vec{r}_i}{dt} = \vec{v}_i$$
$$\frac{d\vec{v}_i}{dt} = \sum_{j\neq i}(\vec{F}_{ij}^{C} + \vec{F}_{ij}^{D} + \vec{F}_{ij}^{R}) = \vec{f}_i \quad (1)$$

The interactions between beads are characterized by pairwise conservative, dissipative, and random forces, which are described as

$$\vec{F}_{ij}^{C} = \alpha_{ij}(1 - r_{ij}/r_c)\vec{e}_{ij}$$
$$\vec{F}_{ij}^{D} = -\gamma w^{D}(r_{ij})(\vec{e}_{ij}\cdot\vec{v}_{ij})\vec{e}_{ij}$$
$$\vec{F}_{ij}^{R} = \sigma w^{R}(r_{ij})\theta_{ij}\vec{e}_{ij} \quad (2)$$

where $\vec{r}_{ij} = \vec{r}_i - \vec{r}_j$, $r_{ij} = |\vec{r}_{ij}|$, $\vec{e}_{ij} = \vec{r}_{ij}/r_{ij}$, $\vec{v}_{ij} = \vec{v}_i - \vec{v}_j$, and r_c, θ_{ij}, α_{ij} is the interaction cutoff radius, a random number with Gaussian distribution and unit variance, and the interaction parameter between beads i and j, respectively.

The relation between the two weight functions $w^{D}(r_{ij})$ and $w^{R}(r_{ij})$ of dissipative and random forces can be described as[36]

$$w^{D}(r_{ij}) = [w^{R}(r_{ij})]^2$$
$$\sigma^2 = 2\gamma k_B T \quad (3)$$

In this work, we set the NPAM (that is, AuNPs tethered with BCPs of PS-*b*-PEO) as a composite system comprising eight linear chains connected to a center NP core. The system was denoted as $C_{90}(A_xB_y)_8$, where A, B, and C_{90} represents the hydrophobic PS, the hydrophilic PEO, and the AuNPs containing 90 CG beads to form a spherical rigid body.[37] Each $C_{90}(A_xB_y)_8$ system contains $N_b = 8(x + y) + 90$ beads, in which x and y are the length of A and B blocks, respectively. We set the cubic box side length as 80, which represents 800 nm in experiment, and control the number density of CG beads at 3. The total number of beads in our simulations is 1 536 000, which contains 125 $C_{90}(A_xB_y)_8$ (that is, NPAMs), 2000 $A_{18}B_1$ free BCPs (that is, MAMs), and the remaining part as water. All simulations are performed in NVT ensemble using GALAMOST[38] on Nvidia Tesla C2050 GPU.

Coarse-Grain Mapping. We chose an appropriate coarse-graining level for water, PEO, PS, and AuNPs in order to correlate our simulation to experiments. The diameter of the rigid body C90 is 2.0 in our simulations, which represents 20 nm AuNP core in experiment. The corresponding CG models of water, PEO, and PS were then determined by this coarse-graining level (see SI for details). We vary the length of A and B blocks as A_3B_1, A_6B_1, $A_{12}B_1$, $A_{14}B_1$, $A_{17}B_1$, $A_{25}B_1$ in our simulations to characterize different lengths of PS block, such as $PS_{54}PEO_{45}$, $PS_{108}PEO_{45}$, $PS_{216}PEO_{45}$, $PS_{252}PEO_{45}$, $PS_{306}PEO_{45}$, $PS_{450}PEO_{45}$ in experiments, respectively. The free BCPs are mapped onto $A_{18}B_1$ in our simulations to characterize $PS_{320}PEO_{45}$ in experiments. Since PEO is miscible with water at almost any concentration and AuNP and PS dislike water, $\alpha_{BS} = 27$, $\alpha_{CS} = 80$, and $\alpha_{AS} = 120$ are used in our simulations. We fix the interaction parameter between the same type of beads at $\alpha_{ii} = 25$ to correctly describe the compressibility of water[35] and set $\alpha_{CB} = \alpha_{AB} = 40$ to describe the incompatibility between Au/PS and PEO components. Koutsos et al. found that the PS chains are weakly adsorbed on the gold substrate, so we set $\alpha_{CA} = 30$.[39]

3. RESULTS AND DISCUSSION

3.1. Self-Assembly of Binary MAMs and NPAMs. The NPAMs used for assembly were prepared by tethering thiol-terminated amphiphilic linear BCPs of HS-PS-*b*-PEO on the surfaces of AuNPs through ligand exchange.[8,11] Free amphiphilic BCPs of PS-*b*-PEO without thiol groups were used as MAMs to coassemble with NPAMs. To optimize the assembly structures, a systematic study was conducted by using different sizes of AuNPs and lengths of individual blocks of tethered and free BCPs. The coassembly system of NPAMs and MAMs was denoted as Au-*D*-PS_{x_1}-*b*-PEO_{y_1}/PS_{x_2}-*b*-PEO_{y_2}, where *D* is the diameter of AuNPs, and x_1, y_1, x_2, and y_2 are the repeating units of individual blocks of tethered and free BCPs, respectively. The characterization details of BCPs are summarized in Table 1.

Table 1. Characterization of Amphiphilic BCPs Used for Self-Assembly[a]

HS-PS_{x_1}-*b*-PEO_{y_1}	x_1	y_1	M_n (kg/mol)^{GPC}	M_n (kg/mol)^{NMR}	PDI
1	114	45	9.7	13.9	1.11
2	211	45	16.0	23.9	1.15
3	245	45	18.1	25.7	1.12
4	304	45	24.0	33.6	1.2
5	455	45	30.2	49.3	1.18
PS_{x_2}-*b*-PEO_{y2}	x_2	y_2	M_n (kg/mol)^{GPC}		PDI
1	307	5	32.2		1.06
2	307	45	34		1.04
3	307	383	49		1.06
4	678	80	73.5		1.10

[a] M_n (kg/mol)^{GPC}: the number-average molecular weight determined by GPC using polystyrene standards for calibration. M_n (kg/mol)^{NMR}: the molecular weight calculated from ^{1}H NMR measurements. PDI stands for polydispersity index.

The coassembly of two types of amphiphiles was triggered by adding water, which is a selective solvent for NPAMs and MAMs, into the binary mixtures of amphiphiles in THF, followed by dialysis against deionized water to remove THF. The assemblies of these binary amphiphiles were hybrid vesicles with various morphologies, namely, JVs (Figure 2a−d), PVs (Figure 2e), and HVs (Figure 2f), depending on the size of NPAMs and the length of constituent blocks of both free and tethered BCPs. Since the BCP tethers and free BCPs were both PS-*b*-PEO, the entropy contribution toward the over free

dx.doi.org/10.1021/ja412172f | J. Am. Chem. Soc. 2014, 136, 2602−2610

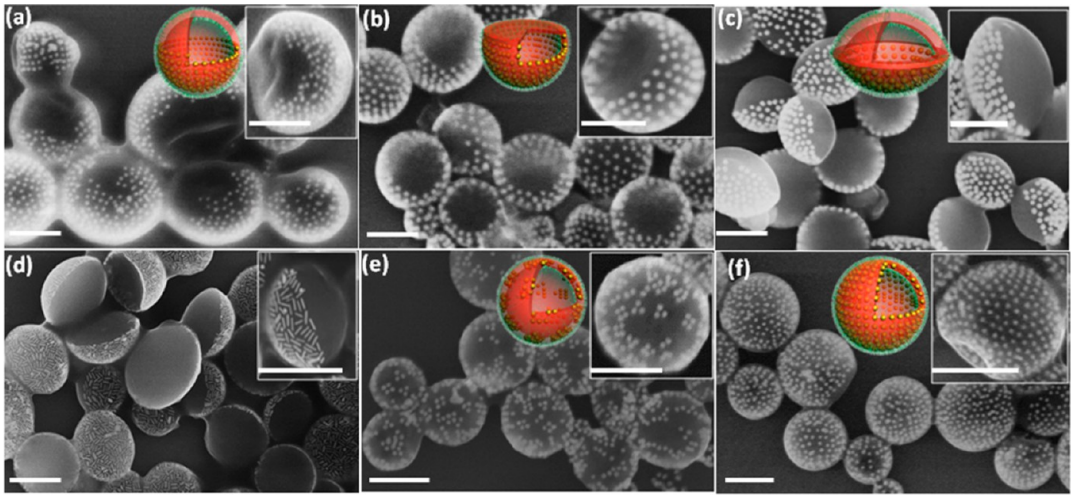

Figure 2. Coassembly of binary mixtures of MAMs and NPAMs into hybrid vesicles. (a–d) Representative SEM images of JVs with spherical (a), hemispherical (b), and disk-like (c,d) shapes. SEM images of PVs (e) and HVs (f). The hybrid vesicles were assembled from a mixture of MAMs and NPAMs: (a) Au-19-PS_{245}-*b*-PEO_{45}/PS_{307}-*b*-PEO_{45}, (b) Au-19-PS_{211}-*b*-PEO_{45}/PS_{307}-*b*-PEO_5, (c) Au-40-PS_{455}-*b*-PEO_{45}/PS_{307}-*b*-PEO_5, (d) Au-40(rods)-PS_{455}-*b*-PEO_{45}/PS_{307}-*b*-PEO_5, (e) Au-19-PS_{114}-*b*-PEO_{45}/PS_{678}-*b*-PEO_{80}, and (f) Au-19-PS_{455}-*b*-PEO_{45}/PS_{307}-*b*-PEO_5. All the self-assemblies were conducted in a water/THF mixture (1:3 in volume ratio). The scale bars: 400 nm in (a), 150 nm in (b), 200 nm in (c,e,f), and 600 nm in (d).

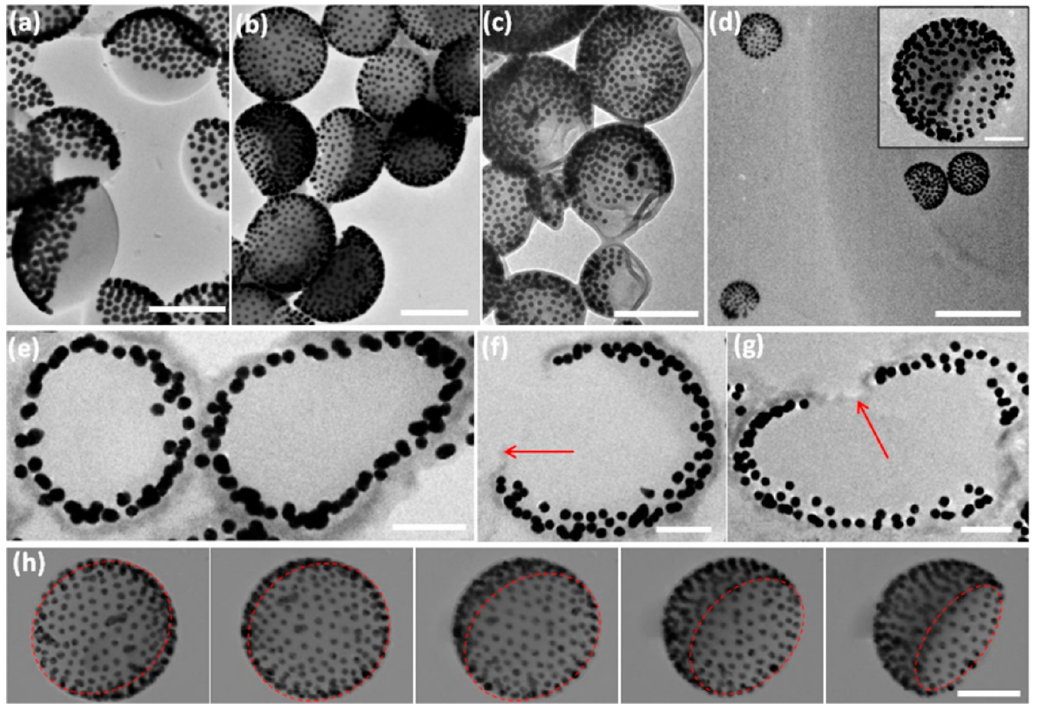

Figure 3. TEM characterization of hybrid JVs. (a–c) Representative TEM images of JVs with disk-like (a), hemispherical (b), and spherical (c) shapes. (d) Cryo-TEM image of hemispherical JVs. (e–g) TEM images of microtome sections of hybrid JVs along different slicing directions: crossing the NPAM half only (e) and crossing both the NPAM and MAM halves (f,g). Red arrow indicates the location of polymer domains in the membranes of vesicles. (h) Tomographic TEM images of JVs at different tilting angles (left to right: −42°, −22°, −2°, 38°, and 50°). Hybrid JVs are assembled from a binary system of (a) Au-40-PS_{455}-*b*-PEO_{45}/PS_{307}-*b*-PEO_5, (b,d,e–h) Au-19-PS_{245}-*b*-PEO_{45}/PS_{307}-*b*-PEO_5, and (c) Au-19-PS_{245}-*b*-PEO_{45}/PS_{307}-*b*-PEO_{45}. All the self-assemblies were conducted in a water/THF mixture (1:3 in volume ratio). The scale bars are 500 nm in (a,d), 300 nm in (b,c), 100 nm in (e–h) and in the inset of (d).

energy gain became critical in the course of assembly. In this case, the nonabsorbing free BCPs (that is, MAMs) served not only as building blocks participating in the assembly but also as depletant to induce short-range attraction between NPAMs due to depletion effect.[29] The depletion interactions excluded the MAMs from pairs of NPAMs and hence increased the conformational entropy of the MAMs, which reduced the overall free energy of the system. This resulted in the lateral phase separation of MAMs with NPAMs within the 2D vesicular membranes. When the MAMs and NPAMs strongly segregated, the assembly produced JVs comprised distinguished halves of the two types of amphiphiles with a sharp boundary (Figure 2a–d). Otherwise, the assembly of binary amphiphiles generated PVs with many small NPAM domains surrounded by a continuous MAM domain (Figure 2e) or HVs with uniform distribution of NPAMs in the membranes (Figure 2f).

dx.doi.org/10.1021/ja412172f | *J. Am. Chem. Soc.* 2014, 136, 2602–2610

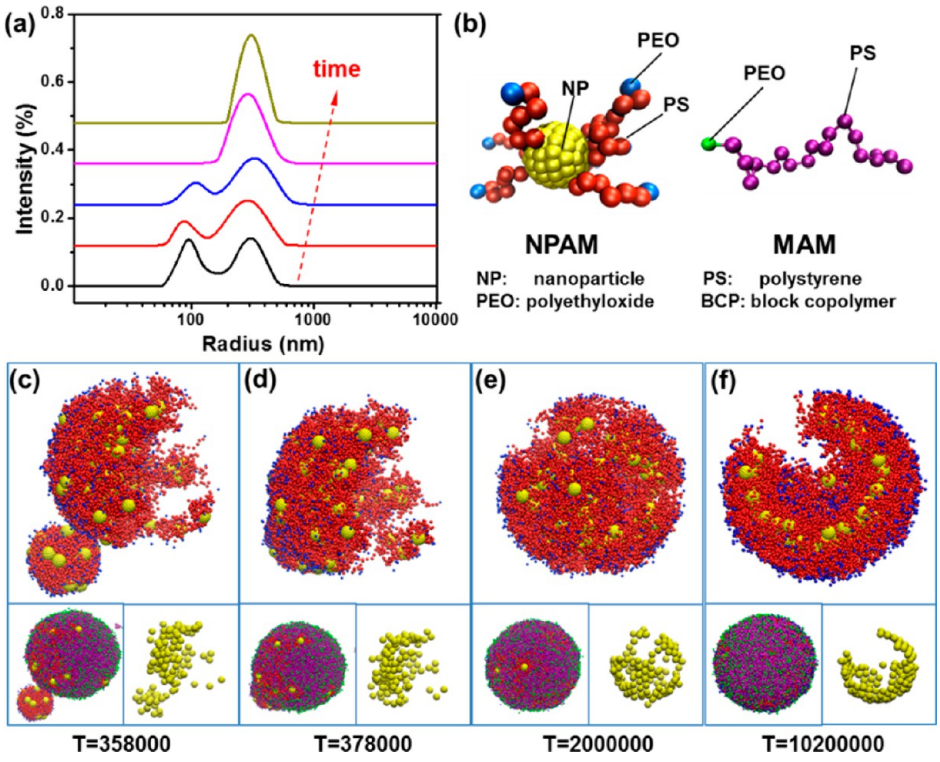

Figure 4. Kinetics of the coassembly of MAMs and NPAMs into hybrid JVs in selective solvents. (a) Time-dependent DLS measurements of the assembly of the two types of amphiphiles after different times of assembly: (from bottom to top) 30, 40, 70, 130, and 190 min after the addition of water to the system. The hybrid vesicles were assembled from Au-19-PS_{211}-*b*-PEO_{45}/PS_{307}-*b*-PEO_5 in a water/THF mixture (1:3 in volume ratio). (b) Schematic illustration of binary amphiphiles used in DPD simulation. (c–f) Snap-shots of DPD-simulated assembly of the binary amphiphiles at different simulation times: T = 358 000 (c), T = 378 000 (d), T = 2 000 000 (e), and T = 10 200 000 (f). Snap-shots show the fusion of NPAM clusters and vesicular assembly and the lateral phase-separation of NPAMs and MAMs in the vesicular membrane to form hybrid JVs.

Nevertheless, the dominant role of entropy in assembly conceptually differs our system from any existing concurrent assembly of pure organic MAMs.

Nonspherical vesicles represent the complexity of lipid-based biological membranes.[1] However, the formation of nonspherical vesicles is rare in a polymer or NP system.[28] Remarkably, the coassembly of binary amphiphiles allows us to tune the shapes of vesicles, thanks to the unique characteristics (i.e., dimension, bending modulus, rigidity) of NPAMs. We ascribe the nonspherical shapes of hybrid JVs to the interplay of bending modules and line tension of multiple domains of NPAMs and MAMs. For example, the assembly of Au-19-PS_{245}-*b*-PEO_{45}/PS_{307}-*b*-PEO_{45} generated JVs with a spherical shape (Figure 2a). When the lengths of free and tethered BCPs were changed, a binary mixture of Au-19-PS_{211}-*b*-PEO_{45}/PS_{307}-*b*-PEO_5 assembled into JVs with hemispherical shape (Figure 2b). The bowl-like body of such vesicles was constructed from the rigid NPAMs, while a nearly flat polymer membrane covered the bowl to form enclosed vesicular compartments (see atomic force microscopy images in Figure S1). When the size of NPAMs (or the NP core of NPAMs) increased, the bending module of NPAM membranes increased. As a result, the curvature of the NPAM membranes decreased to release the bending energy, resulting in the formation of disk-like hybrid JVs with two symmetric halves for the Au-40-PS_{455}-*b*-PEO_{45}/PS_{307}-*b*-PEO_5 system (Figure 2c,d).[40] The exact mechanism is still unclear and needs further exploration in future research.

3.2. Structural Characterizations of Hybrid JVs. The hybrid JVs constituted a hollow interior constructed from binary mixtures of amphiphiles with significantly different dimensions, geometries, and compositions. The NPAM half of hybrid JVs was made from a monolayer of densely packed AuNPs with relatively uniform spacing (Figure 3a–c). Taking hemispherical hybrid JVs assembled from Au-19-PS_{245}-*b*-PEO_{45}/PS_{307}-*b*-PEO_5 system as an example (Figure 3b), we characterized the hollow interior and Janus-like morphology of the vesicles using various TEM techniques (Figure 3d–h).

First, cryogenic TEM (cryo-TEM) image clearly showed the presence of hemispherical vesicles with a single layer of AuNPs in solution (Figure 3d). Second, the hollow feature was demonstrated by the ring-like array of AuNPs in microtome sections of JVs (Figure 3e–g). Depending on the slicing direction of JVs, the cross-section of JVs appeared as either a completely closed ring (Figure 3e) or a nonclosed ring with an opening (that is, a portion with the absence of AuNPs) which was corresponding to the MAM domain of hybrid JVs (Figure 3f,g). The membrane thicknesses of the MAM and NPAM domains were roughly estimated to be ~20.8 and ~39.1 nm, respectively. The single array of AuNPs in the rings further confirmed that the NPAM domains of the vesicles consisted of a single layer of densely packed AuNPs. Third, electron microscopy tomography was used to record TEM images of HJVs at multiple tilt angles (−42° to 50°) (Figure 3h). A series of tomographic TEM images illustrated the orientations of JVs with the MAM domain facing different directions (see supporting Movie 1). In addition, a close inspection of JVs with intact and broken membranes of the polymer half further confirmed the hollow cavity of the vesicles as well as the

dx.doi.org/10.1021/ja412172f | J. Am. Chem. Soc. 2014, 136, 2602–2610

presence of the polymer domain in the vesicular membranes (Figures S8 and S9).

The surface area ratio of the two halves of hybrid JVs can be readily controlled by tuning the ratio of the two types of amphiphiles. We varied the concentration of NPAMs in the mixture, while keeping the amount of MAMs as a constant. With the increase of NPAM concentration from 0.21, to 0.45, and to 0.90 mg/mL, the surface fraction of NPAM half in hybrid JVs increased from 27.4%, to 38.1%, and to 85.9% (Figure S10). The JVs maintained a hemispherical shape, while varying the surface fraction of two halves.

3.3. Experimental and Computational Studies on Assembly Kinetics. We studied the kinetics of the formation process of hybrid JVs using a system of Au-19-PS_{211}-*b*-PEO_{45}/PS_{307}-*b*-PEO_5 as an example. Time-dependent dynamic light scattering (DLS) measurement showed the evolution of hydrodynamic radius (R_h) of the assemblies in the mixed solvents (Figure 4a). About 30 min after the addition of water, two populations of assemblies with R_h of ~91.5 and ~299.5 nm were presented in the system. They corresponded to small clusters of NPAMs and relatively big vesicles with randomly distributed MAMs and NPAMs in the membranes, as confirmed by SEM characterization (Figure S11a). With time, the population of clusters gradually decreased, accompanied with an increase in the diameter of vesicles (Figure 4a, and Figure S11c). This can be explained by the fusion of clusters with vesicles, in order to reduce the unfavorable exposure of hydrophobic constituents of small clusters of NPAMs and hence minimize the overall interfacial free energy of the system. About 130 min after the addition of water, only one population of assemblies with R_h of ~313 nm was presented in the system. The NPAMs within the vesicular membranes laterally migrated and packed more closely to each other, resulting in the formation of hybrid JVs with distinguished two halves. In a word, the concurrent assembly involves three critical steps, namely, initiation of assembly, fusion of nanostructures, and phase separation of two types of amphiphiles within membranes. (Figure S11).

We simulated the coassembly of binary amphiphiles by dissipative particle dynamics (DPD),[35,38] using a CG model (see details of models in SI).[32,34] Note that our simulation model did not take into account the shapes of vesicles at present stage. Figure 4b illustrates the model of NPAMs containing AuNP cores tethered with amphiphilic linear BCPs, and MAMs of free BCPs (see Tables S1 and S2 for details). Our simulation confirmed the three critical steps of the formation of HJVs. Snap-shots of the simulation in Figure 4c–f clearly show the fusion of NPAM clusters with vesicular assemblies and the subsequent phase separation of binary amphiphiles within individual vesicles. We noticed that the fusion of the clusters and vesicles took place rapidly in the simulation. In contrast, the lateral phase separation of binary mixtures of amphiphiles was rather slow to rearrange their organization in the membranes, due to the slow diffusion rate of relatively large NPAMs.

3.4. Phase Separation Behaviors of Binary Mixtures of Amphiphiles Confined in the Vesicular Membranes. The phase separation behaviors of assembly of two types of amphiphiles as well as resulting assembly morphologies were strongly dependent on the relative length of individual blocks of free and tethered BCPs. The results of our systematic study were summarized in a phase-like diagram in Figure 5a. First of all, the PS length of tethered BCPs of NPAMs played a critical

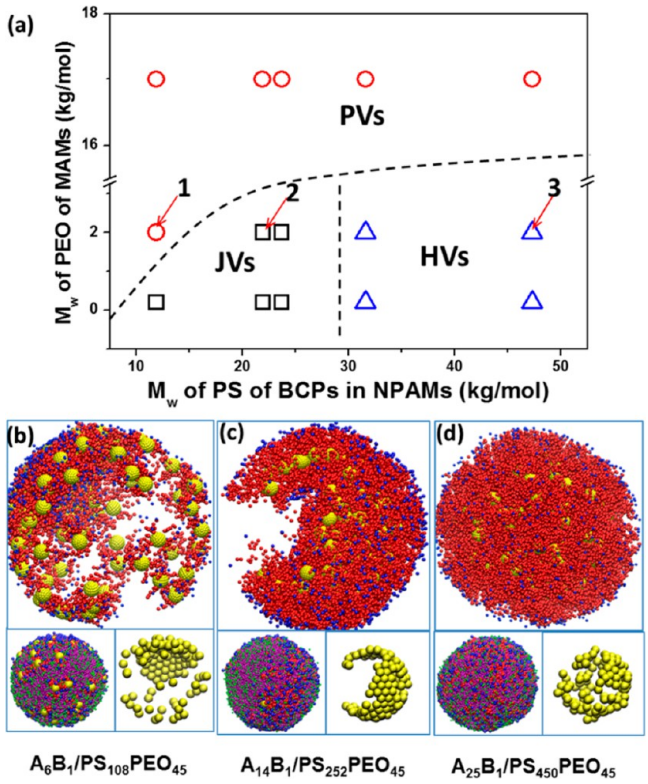

Figure 5. Phase separation behavior between the amphiphiles of MAMs and NPAMs. (a) Phase-like diagram of experimental study of the assembly of the two types of amphiphiles in a water/THF mixture (1:3 in volume ratio). In all conditions, the diameters of AuNPs in NPAMs were ~19 nm. PEO blocks of BCPs in NPAMs were 2 kDa, while the PS blocks of MAMs were 32 kDa. Binary mixtures for the points 1–3 in the phase-like diagram are Au-19-PS_{114}-*b*-PEO_{45}/PS_{307}-*b*-PEO_{45}, Au-19-PS_{211}-*b*-PEO_{45}/PS_{307}-*b*-PEO_{45}, and Au-19-PS_{455}-*b*-PEO_{45}/PS_{307}-*b*-PEO_{45}. (b–d) Snap-shots of DPD simulation of coassembly systems corresponding to points 1–3 in (a). For visualization purpose, MAMs are not shown in the top images in (b–d), and only AuNPs are shown in the right bottom images in (b–d).

role in the phase separation of binary amphiphiles during assembly. Taking binary system with MAMs of PS_{307}-*b*-PEO_5 (M_w of PS is 32 kDa and M_w of PEO is 200 Da) as an example, when the PS length of tethered BCPs was relatively short (i.e., a M_w of 11.9, 21.9, and 23.7 kDa), a strong phase separation between binary amphiphiles occurred to generate hybrid JVs with two distinguished halves (Figures 5a and S12a,b). When the PS length of tethered BCPs was long (i.e., a M_w of 31.6 and 47.3 kDa), NPAMs were uniformly distributed in the MAM membrane to form hybrid HVs (Figure S12c,d). In this case, the interparticle spacing between AuNPs within assemblies of binary amphiphiles was 16 nm, which was much larger than 9 nm for that of pure NPAM assembly system. This indicated that the MAMs were filled in-between NPAMs within vesicular membranes. Second, the PEO length of MAMs also influenced the morphologies of assemblies of the two types of amphiphiles. For a system with Au-19-PS_{211}-*b*-PEO_{45} as NPAMs, when MAMs with short PEO blocks (i.e., a M_w of 0.2 and 2 kDa) were used, the binary mixture of amphiphiles strongly segregated in the membranes to generate JVs. For MAMs with longer PEO blocks (i.e., M_w of 17 kDa) were used, their coassembly with NPAMs carrying any length of tethered BCPs produced PVs with many small NPAM domains

dx.doi.org/10.1021/ja412172f | J. Am. Chem. Soc. 2014, 136, 2602–2610

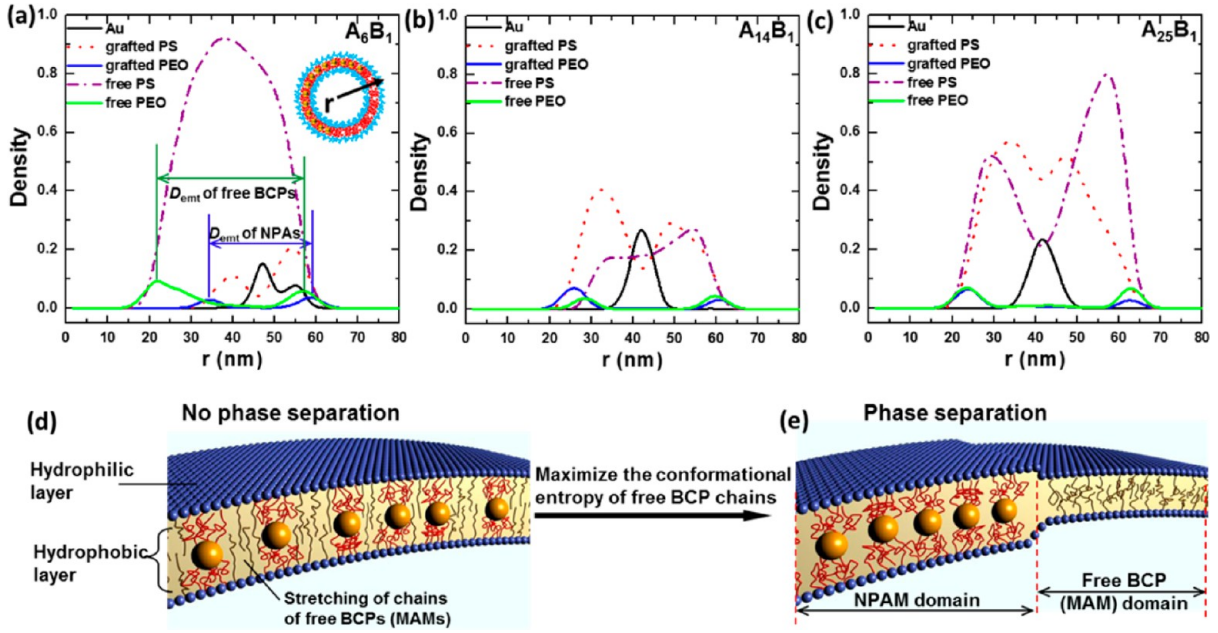

Figure 6. Membrane structures of the vesicles assembled from binary mixtures of amphiphiles of MAMs and NPAMs. (a–c) RDD of each component of assembly of two types of amphiphiles corresponding to points 1–3 in the phase-like diagram in Figure 5: PVs (a), JVs (b), and HVs (c). Length of PS blocks of MAMs and PEO blocks of tethered BCPs is 32 and 2 kDa, respectively. AuNPs with a diameter of 19 nm were used in all experiments. (d,e) Schematic illustration of the formation mechanism of hybrid JVs due to phase separation. (d) In membrane without phase separation, the MAMs are stretched in the direction normal to the membrane due to the compression from neighboring NPAMs. (e) Effective attraction between NPAMs is induced by the need for maximizing conformational entropy of MAMs.

surrounded by a continuous phase of MAMs in the membranes. Our DPD simulation results were in good agreement with the experimental observations. The assemblies transited from PVs, to JVs, and to HVs eventually, when the PS length of tethered BCPs increased from 11.9 to 47.3 kDa (Figure 5b–d). All the assembled structures observed in our experiments and simulations are reproducible, which manifests the stability of JV, PV, and HV characteristics. This also implies that the observed structures are equilibrium structures.

Our simulation results showed more details on the vesicle structures and the driving force of phase separation. We radially sliced the space with constant distance starting from the center of mass of the vesicle and defined radial density distributions (RDDs) of one component as the number of the specific component divided by the volume of the spherical shell. Figure 6a–c show the RDDs of each component of assemblies with different morphologies. The appearance of two distinguished peaks for hydrophilic PEO (or hydrophobic PS) in all the systems indicated that AuNPs were sandwiched between two hydrophilic PEO (or hydrophobic PS) layers which form the internal and external surfaces of the vesicle. We calculated the effective membrane thickness (D_{emt}) of each type of amphiphiles in the vesicle by using the distance between the two peaks of PEO blocks (Table 2). For both phase separated systems (hybrid PVs and JVs), D_{emt} of NPAMs was significantly different from that of MAMs, that is, 22.4 and 35.6 nm for patchy system and 26.2 and 20.9 nm for Janus system, while D_{emt} of NPAMs and MAMs in HVs was approximately equal (Figure 6a–c and Table 2). This indicates that the mismatch in D_{emt} of two types of amphiphiles exists in the vesicular membranes with surface patterns, which can be explained by the unique role of entropy during assembly. If the vesicle membrane comprises randomly distributed NPAMs and MAMs, then MAMs will be stretched in the direction normal to the membrane, due to the compression from neighboring NPAMs (Figure 6d). The stretching constraint on chain conformations of MAMs will be reduced by grouping MAMs together to form a large domain of their own, in which the MAM chains possess larger conformational entropy (Figure 6e). Although membrane thickness mismatch is energetically unfavorable to form hybrid JVs, the accompanied chain conformational entropy increases largely in MAM domain, which decreases overall free energy and favors the formation of hybrid JVs.

Table 2. Effective Membrane Thickness (D_{emt}) of MAM and NPAM Domains

model in simulations	A_6B_1	$A_{14}B_1$	$A_{25}B_1$
chain length	$PS_{108}PEO_{45}$	$PS_{252}PE0_{45}$	$PS_{450}PEO_{45}$
D_{emt} of NPAMs (nm)	22.4 ± 0.6	36.2 ± 0.6	40.4 ± 1.1
D_{emt} of free BCPs (nm)	35.6 ± 0.3	30.9 ± 0.6	40.4 ± 1.1

Simulation of the dynamics of assembly process indicated that both the mobility of NPAMs and the entanglement of polymer chains influenced the final morphology of assembled structures. When NPAMs carrying short BCPs (PS_{108}-*b*-PEO_{45}) were assembled with MAMs of PS_{307}-*b*-PEO_{45}, the NPAMs migrated rapidly within the membrane, resulting in the fluctuation of the domain boundaries in the membranes (see supporting Movie 2). Small NPAM domains continuously merged into larger domains, while these large domains could not maintain a stable packing state and slowly dissociated into small individuals. In this case, hybrid PVs were formed as shown in both our experiments and simulations. This observation is also reflected by the presence of two distinguished RDD peaks of AuNPs (Figure 6a): AuNPs were frequently pulled toward the outer or inner leaflet of the

dx.doi.org/10.1021/ja412172f | J. Am. Chem. Soc. 2014, 136, 2602–2610

vesicle, rather than being stabilized in the center of the vesicular membrane as in hybrid JVs.

Alternatively, hybrid PVs can be produced when the chain length of hydrophilic PEO block (of MAMs) is significantly increased, as shown in Figure 5a. When we increased the PEO length of MAMs 1 order of magnitude, the MAMs in membranes were largely stretched due to the tendency of solvation of PEO blocks in water. This resulted in larger D_{emt} of MAMs. In contrast, the D_{emt} due to the variation of PS block length in NPAMs did not change that much, since PS blocks can be considered as in melt phase. Thus the AuNPs (of NPAMs) were mainly distributed in the outer or inner leaflet of the vesicular membrane (rather than in the center of the membrane). As a result, the mobility of NPAMs significantly increases, thus favoring the formation of PVs. This explains the formation of PVs for large PEO block length in the MAMs, regardless of the length of the PS block in the NPAMs. This also explains the transition from HVs to PVs in Figure 5a.

When NPAMs carrying very long BCPs (PS_{450}-*b*-PEO_{45}) were used, the entanglement of long polymer chains significantly reduced the mobility of NPAMs (see supporting Movie 3). The highly localized motion of NPAMs led to the uniform distribution of NPAMs within a continuous phase of MAMs in the membranes of HVs. The homogeneous distribution of NPAMs in vesicle in turn induced the stretching of MAM chains, as indicated by the equal value (40.4 nm) of D_{emt} and the overlap of the RDD along radical direction for both amphiphiles (Figure 6c). In this case, although the conformational entropy of MAMs was reduced, the increase in the translational entropy of AuNPs favored the homogeneous distribution of AuNPs in the vesicle. In addition, the stretching of MAMs enhanced the lateral packing (or interactions) of the grafted BCP chains and free BCP chains and reduced the roughness of the inner and outer surface of vesicular membranes, thus giving rise to a lower overall interfacial free energy of the system.

In a word, the mismatch of PS chain length, the entanglement of polymer chains, and the mobility of NPAMs synergistically determine the three types of morphologies of vesicular assemblies. The hybrid JVs only formed when the lengths of free BCPs of MAMs and tethered BCPs in NPAMs were in a specific window, as shown in Figure 5a (see supporting Movie 4). The need for maximizing conformational entropy of polymers induces effective attraction between NPAMs, thus leading to a well-equilibrated Janus structure under thermodynamic control. For the formation of PVs and HVs, other than dominant role of thermodynamics, the assembly is also affected by kinetic factors (i.e., entanglement of polymer chains).

4. CONCLUSIONS

In summary, we demonstrated a simple yet powerful strategy for designing hybrid vesicles with well-defined shape, morphology, and surface pattern through coassembly of multiple types of amphiphiles. The dominant role of entropy in the coassembly process conceptually differs our system from any existing concurrent assembly of solely organic amphiphiles. These hybrid vesicles have potential applications in sensing,[41] bioimaging,[42] drug delivery,[17] nano- and microreactors,[43] and optoelectronics.[44] The ability to construct discrete nanostructures from multiple types of amphiphiles with distinct size, shape, and composition paves the way for the fabrication of structurally complex functional materials with broad applications. Moreover, this strategy will significantly enlarge the library of tunable parameters (i.e., dimension, shape, rigidity, bending modulus, etc.) available for controlling assembly, which is unattainable solely by organic amphiphiles.

■ ASSOCIATED CONTENT

Supporting Information

Details of simulation, surface coverage calculations and corresponding SEM images, AFM images, large area SEM and TEM images, UV and DLS of spectrum, and SEM images of kinetic studies are available. This information is available free of charge via the Internet at http://pubs.acs.org.

■ AUTHOR INFORMATION

Corresponding Authors

luzhy@jlu.edu.cn
znie@umd.edu

Notes

The authors declare no competing financial interest.

■ ACKNOWLEDGMENTS

This work is supported by NSF Career Award (DMR-1255377) and NSFC (21025416). We thank Prof. Lawrence Sita and Wonseok Hwang for GPC measurement, Prof. Mikhail A. Anisimov, Dr. Deepa Subramanian, and Prof. Srinivasa R. Raghavan for DLS measurement, Prof. Peter Kofinas and Dr. Xin Zhang for help on microtome, and Dr. Wen-An Chiou and Dr. Panju Shang for technical assistance on TEM imaging. We acknowledge the support of Maryland NanoCenter and its NispLab. The NispLab is supported in part by the NSF as a MRSEC Shared Experimental Facilities.

■ REFERENCES

(1) Subramaniam, A. B.; Guidotti, G.; Manoharan, V. N.; Stone, H. A. *Nat. Mater.* **2013**, *12*, 128.
(2) Discher, D. E.; Eisenberg, A. *Science* **2002**, *297*, 967.
(3) Zhang, X.; Wang, C. *Chem. Soc. Rev.* **2011**, *40*, 94.
(4) Mai, Y.; Eisenberg, A. *Chem. Soc. Rev.* **2012**, *41*, 5969.
(5) Zhang, S. G. *Nat. Biotechnol.* **2003**, *21*, 1171.
(6) Cui, H.; Chen, Z.; Zhong, S.; Wooley, K. L.; Pochan, D. J. *Science* **2007**, *317*, 647.
(7) Song, J.; Cheng, L.; Liu, A.; Yin, J.; Kuang, M.; Duan, H. *J. Am. Chem. Soc.* **2011**, *133*, 10760.
(8) He, J.; Huang, X.; Li, Y.-C.; Liu, Y.; Babu, T.; Aronova, M. A.; Wang, S.; Lu, Z.; Chen, X.; Nie, Z. *J. Am. Chem. Soc.* **2013**, *135*, 7974.
(9) Moffitt, M. G. *J. Phys. Chem. Lett.* **2013**, *4*, 3654.
(10) Nie, Z.; Fava, D.; Kumacheva, E.; Zou, S.; Walker, G. C.; Rubinstein, M. *Nat. Mater.* **2007**, *6*, 609.
(11) He, J.; Liu, Y.; Babu, T.; Wei, Z.; Nie, Z. *J. Am. Chem. Soc.* **2012**, *134*, 11342.
(12) He, J.; Wei, Z. J.; Wang, L.; Tomova, Z.; Babu, T.; Wang, C. Y.; Han, X. J.; Fourkas, J. T.; Nie, Z. H. *Angew. Chem., Int. Ed.* **2013**, *52*, 2463.
(13) Guo, Y.; Harirchian-Saei, S.; Izumi, C. M. S.; Moffitt, M. G. *ACS Nano* **2011**, *5*, 3309.
(14) Hu, J.; Wu, T.; Zhang, G.; Liu, S. *J. Am. Chem. Soc.* **2012**, *134*, 7624.
(15) He, J.; Zhang, P.; Babu, T.; Liu, Y.; Gong, J.; Nie, Z. *Chem. Commun.* **2013**, *49*, 576.
(16) Nie, Z.; Petukhova, A.; Kumacheva, E. *Nat. Nanotechnol.* **2010**, *5*, 15.
(17) Lin, J.; Wang, S.; Huang, P.; Wang, Z.; Chen, S.; Niu, G.; Li, W.; He, J.; Cui, D.; Lu, G.; Chen, X.; Nie, Z. *ACS Nano* **2013**, *7*, 5320.
(18) Lee, J.; Hernandez, P.; Lee, J.; Govorov, A. O.; Kotov, N. A. *Nat. Mater.* **2007**, *6*, 291.

(19) Huynh, W. U.; Dittmer, J. J.; Alivisatos, A. P. *Science* **2002**, *295*, 2425.
(20) Maier, S. A.; Kik, P. G.; Atwater, H. A.; Meltzer, S.; Harel, E.; Koel, B. E.; Requicha, A. A. G. *Nat. Mater.* **2003**, *2*, 229.
(21) Zheng, R. H.; Liu, G. J.; Yan, X. H. *J. Am. Chem. Soc.* **2005**, *127*, 15358.
(22) Christian, D. A.; Tian, A.; Ellenbroek, W. G.; Levental, I.; Rajagopal, K.; Janmey, P. A.; Liu, A. J.; Baumgart, T.; Discher, D. E. *Nat. Mater.* **2009**, *8*, 843.
(23) Groeschel, A. H.; Schacher, F. H.; Schmalz, H.; Borisov, O. V.; Zhulina, E. B.; Walther, A.; Mueller, A. H. E. *Nat. Commun.* **2012**, *3*, 710.
(24) Rupar, P. A.; Chabanne, L.; Winnik, M. A.; Manners, I. *Science* **2012**, *337*, 559.
(25) Glotzer, S. C.; Solomon, M. J. *Nat. Mater.* **2007**, *6*, 557.
(26) Shields, C. W.; Zhu, S.; Yang, Y.; Bharti, B.; Liu, J.; Yellen, B. B.; Velev, O. D.; Lopez, G. P. *Soft Matter* **2013**, *9*, 9219.
(27) Schulz, M.; Glatte, D.; Meister, A.; Scholtysek, P.; Kerth, A.; Blume, A.; Bacia, K.; Binder, W. H. *Soft Matter* **2011**, *7*, 8100.
(28) Zhu, J.; Zhang, S.; Zhang, K.; Wang, X.; Mays, J. W.; Wooley, K. L.; Pochan, D. J. *Nat. Commun.* **2013**, *4*, 2297.
(29) Sacanna, S.; Irvine, W. T. M.; Chaikin, P. M.; Pine, D. J. *Nature* **2010**, *464*, 575.
(30) Frens., G. *Nat. Phys. Sci.* **1973**, *241*, 20.
(31) Groot, R. D.; Madden, T. J. *J. Chem. Phys.* **1998**, *108*, 8713.
(32) Qian, H. J.; Lu, Z. Y.; Chen, L. J.; Li, Z. S.; Sun, C. C. *Macromolecules* **2005**, *38*, 1395.
(33) Pons-Siepermann, I. C.; Glotzer, S. C. *ACS Nano* **2012**, *6*, 3919.
(34) Pons-Siepermann, I. C.; Glotzer, S. C. *Soft Matter* **2012**, *8*, 6226.
(35) Groot, R. D.; Warren, P. B. *J. Chem. Phys.* **1997**, *107*, 4423.
(36) Espanol, P.; Warren, P. *Europhys. Lett.* **1995**, *30*, 191.
(37) Nguyen, T. D.; Phillips, C. L.; Anderson, J. A.; Glotzer, S. C. *Comput. Phys. Commun.* **2011**, *182*, 2307.
(38) Zhu, Y. L.; Liu, H.; Li, Z. W.; Qian, H. J.; Milano, G.; Lu, Z. Y. *J. Comput. Chem.* **2013**, *34*, 2197.
(39) Koutsos, V.; vanderVegte, E. W.; Pelletier, E.; Stamouli, A.; Hadziioannou, G. *Macromolecules* **1997**, *30*, 4719.
(40) Hu, J.; Weikl, T. R.; Lipowsky, R. *Soft Matter* **2011**, *7*, 6092.
(41) Swierczewska, M.; Liu, G.; Lee, S.; Chen, X. Y. *Chem. Soc. Rev.* **2012**, *41*, 2641.
(42) Chen, J.; Yang, M.; Zhang, Q.; Cho, E. C.; Cobley, C. M.; Kim, C.; Glaus, C.; Wang, L. V.; Welch, M. J.; Xia, Y. *Adv. Funct. Mater.* **2010**, *20*, 3684.
(43) Kim, K. T.; Cornelissen, J. J. L. M.; Nolte, R. J. M.; van Hest, J. C. M. *Adv. Mater.* **2009**, *21*, 2787.
(44) Soukoulis, C. M.; Linden, S.; Wegener, M. *Science* **2007**, *315*, 47.